ATP-Induced Ca^{2+} Release in Cochlear Outer Hair Cells: Localization of an Inositol Triphosphate-Gated Ca^{2+} Store to the Base of the Sensory Hair Bundle

Fabio Mammano,[1] **Gregory I. Frolenkov,**[2] **Laura Lagostena,**[1] **Inna A. Belyantseva,**[2] **Mauricio Kurc,**[2] **Valerie Dodane,**[2] **Alberto Colavita,**[3] **and Bechara Kachar**[2]

[1]*Biophysics Sector and Istituto Nazionale di Fisica della Materia Unit, International School for Advanced Studies, 34014 Trieste, Italy,* [2]*Section on Structural Cell Biology, National Institute on Deafness and Other Communication Disorders, National Institutes of Health, Bethesda, Maryland 20892-4163, and* [3]*Microprocessor Laboratory, Abdus Salam Centre for Theoretical Physics and Istituto Nazionale di Fisica Nucleare, 34014 Trieste, Italy*

We used a high-performance fluorescence imaging system to visualize rapid changes in intracellular free Ca^{2+} concentration ([Ca^{2+}]$_i$) evoked by focal applications of extracellular ATP to the hair bundle of outer hair cells (OHCs): the sensory–motor receptors of the cochlea. Simultaneous recordings of the whole-cell current and Calcium Green-1 fluorescence showed a two-component increase in [Ca^{2+}]$_i$. After an initial entry of Ca^{2+} through the apical membrane, a second and larger, inositol triphosphate (InsP$_3$)-gated, [Ca^{2+}]$_i$ surge occurred at the base of the hair bundle. Electron microscopy of this intracellular Ca^{2+} release site showed that it coincides with the localization of a unique system of endoplasmic reticulum (ER) membranes and mitochondria known as Hensen's body. Using confocal immunofluorescence microscopy, we showed that InsP$_3$ receptors share this location. Consistent with a Ca^{2+}-mobilizing second messenger system linked to ATP-P2 receptors, we also determined that an isoform of G-proteins is present in the stereocilia. Voltage-driven cell shape changes and nonlinear capacitance were monitored before and after ATP application, showing that the ATP-evoked [Ca^{2+}]$_i$ rise did not interfere with the OHC electromotility mechanism. This second messenger signaling mechanism bypasses the Ca^{2+}-clearance power of the stereocilia and transiently elevates [Ca^{2+}]$_i$ at the base of the hair bundle, where it can potentially modulate the action of unconventional myosin isozymes involved in maintaining the hair bundle integrity and potentially influence mechanotransduction.

Key words: sensory transduction; cochlea; purinergic receptors; InsP$_3$; endoplasmic reticulum; mitochondria; G-proteins; electromotility; patch-clamp; calcium imaging; organ of Corti; Hensen's body

Hearing in mammals relies on two types of sensory receptors, the inner and the outer hair cells of the organ of Corti in the cochlea. The defining feature of sensory hair cells is the hair bundle, the mechanoelectrical sensory organelle. Hair cells convert mechanical stimuli into membrane potential variations by activation of mechanosensitive transduction channels located on the stereocilia in the hair bundle (Hudspeth, 1997). Outer hair cells (OHCs) are additionally capable of a motor activity, converting membrane potential variations into cell shape changes at acoustic frequencies, a property generally defined as electromotility (Kachar et al., 1986; Frolenkov et al., 1998) and presumed to be the force-generating mechanism for cochlear amplification.

The mechanosensitive transduction channels of hair cells are nonselective to monovalent cations and permeable to Ca^{2+} (Chabbert et al., 1994; Lumpkin et al., 1997). Ca^{2+} is critical for mechanosensory adaptation in hair cells (Ricci and Fettiplace, 1998) and is also probably involved in the regulation of OHC electromotility (Dallos et al., 1997). Beside mechanosensitive channels, hair cells express ATP-activated P2 purinergic receptors on their stereociliary membrane, which faces the endolymphatic fluid compartment of the cochlea (Mockett et al., 1994). It has recently been proposed that ATP may act as a signaling molecule to modulate receptor function in the cochlea (Housley, 1997; Skellet et al., 1997). When injected into the endolymphatic compartment of the guinea pig cochlea, ATP had a significant effect on gross cochlear potentials (Muñoz et al., 1995) and on electrically-evoked otoacoustic emissions (Kirk and Yates, 1998), two macroscopic correlates of sensory function in the organ of Corti.

Two structurally unrelated families of P2-ATP receptors have been identified: P2X, ionotropic receptors and P2Y, G-protein-coupled (metabotropic) receptors; however, a problem that continues to hinder the study of P2 receptors is the lack of family-selective receptor antagonists (Linden, 1999). In isolated sensory hair cells, application of ATP to the stereocilia has been shown electrophysiologically to gate high-conductance, nonselective cation channels (P2X receptors) that, similar to the mechanosensitive channels, are also permeable to Ca^{2+} (Housley, 1997). Conventional Ca^{2+}-imaging studies showed slow rises of [Ca^{2+}]$_i$

within the OHC cytoplasm peaking in 20–150 sec (Ashmore and Ohmori, 1990; Nilles et al., 1994) after ATP application. In addition, in a biochemical assay, a Ca^{2+}-mobilizing inositol triphosphate (InsP$_3$)-mediated second messenger system, linked to P2Y receptors, was reported in the guinea pig organ of Corti (Niedzielski and Schacht, 1992). Although the role of ATP as a signaling molecule for OHCs remains undetermined, its ability to affect membrane conductance and [Ca^{2+}]$_i$ makes it a likely key factor in the modulation of the cell sensory–motor activity.

We used a high-performance fluorescence imaging system to analyze, at high space and time resolution, the ATP-activated Ca^{2+} signals in OHCs of the guinea pig organ of Corti. We also used confocal immunofluorescence microscopy to obtain evidence that an ATP-activated intracellular Ca^{2+} release is linked to an InsP$_3$-gated intracellular store located at the base of the hair bundle. In an attempt to determine the functional role of this pathway, we monitored the voltage-driven cell shape changes before and after ATP application, showing that the ATP-evoked [Ca^{2+}]$_i$ rise did not interfere with the OHC electromotility mechanism. Our results suggest that, by focally releasing Ca^{2+} from an intracellular store via the long-range intracellular messenger InsP$_3$, ATP can bypass the efficient Ca^{2+}-clearance mechanisms of the stereocilia and thus directly influence the hair bundle mechanosensory functions.

MATERIALS AND METHODS

Cell preparation. Adult guinea pigs (200–400 gm) were anesthetized with carbon dioxide and decapitated. The temporal bones were removed from the skull and placed in modified Leibowitz cell culture medium (L-15) containing (in mM): NaCl, 137; KCl, 5.36; CaCl$_2$, 1.25; MgCl$_2$, 1.0; Na$_2$HPO$_4$, 1.0; KH$_2$PO$_4$, 0.44; and MgSO$_4$, 0.81. For some experiments Ca^{2+} ions were excluded, and the solution was supplemented by 2 mM EGTA (referred to as 0 [Ca^{2+}]$_o$ conditions in the text). pH was adjusted to 7.35 with NaOH and osmolarity to 320 ± 2 mOsm/l with D-glucose. Ca^{2+} imaging experiments were conducted on cells in the whole organ of Corti, using an isolated cochlea preparation, as previously described (Mammano et al., 1995), whereas isolated OHCs were used in the experiments requiring the measurement of cell motility. In the latter case, the bulla was opened to expose the cochlea, and the otic capsule was chipped away with a surgical blade, starting from the base. Strips of the organ of Corti were dissected from the modiolus with a fine needle and transferred with a glass pipette to a 100 μl drop of L-15 medium placed on a microscope slide. Cells were dissociated by reflux of the tissue through the needle of a Hamilton syringe (number 705, 22 gauge) and allowed to settle on the slide for 5–10 min. Thereafter cells were placed in a laminar flow bath (100 μl), where exchange of all solution (>300 μl min) was achieved by gravity feed. Unless explicitly stated, all drugs were purchased from Sigma (St. Louis, MO).

Patch-clamp recordings and drug delivery. Conventional whole-cell patch-clamp recordings were made under visual control after mounting the recording chamber on a microscope stage. OHCs were visualized, and the following morphological features were used to determine viability: uniform cylindrical shape, basal location of the nucleus, membrane birefringence, and intact stereocilia. Cells used in this study ranged in length from 40–70 μm and were maintained at room temperature (22–24°C) throughout the experiment. An Axopatch 1-D amplifier (Axon Instruments, Foster City, CA) was used to drive pipettes that had been pulled on a two-stage vertical puller (PP-83; Narishige, Tokyo, Japan) from 1.5 mm outer diameter soda glass (Clark Electromedical Instruments, Pangbourne, UK). Current and voltage were sampled at either 2.5 or 100 kHz using a standard laboratory interface (Digidata 1200A; Axon Instruments) controlled by pClamp 7.0 software (Axon Instruments). Pipettes were filled with an intracellular solution containing (in mM): KCl, 150; MgCl$_2$, 2.0; EGTA 0.5; Na$_2$HPO$_4$ 8.0; and NaH$_2$PO$_4$ 1.0, adjusted to pH 7.2 with KOH and brought to 320 mOsm/l with D-glucose. To avoid leakage of ATP during seal formation, no ATP was included in the intracellular solution. Over the course of several minutes, this may have caused intracellular ATP to diminish, reducing the ability of the cell to extrude Ca^{2+} and/or to replenish the intracellular stores through the action of the Ca^{2+} ATPases of the soma, hair bundle, and intracellular

stores. To minimize such potentially adverse effects, fluorescence images were generally captured within 3–4 min from achieving the whole-cell patch-clamp configuration. For fluorescence imaging (see below), pipettes were filled with the cell-impermeable form of the Ca^{2+}-selective fluorescent dye Calcium Green-1 (100 μM; C-3010; Molecular Probes, Eugene, OR) dissolved in the intracellular solution described above. Potentials were not corrected for liquid-junction potentials (expected to be approximately −4 mV). The pipette resistance was typically 3 MΩ when measured in the bath. A puff pipette, prepared similarly to the patch pipette and filled with ATP dissolved in the extracellular solution, was placed near the cell stereocilia, and pressure was applied at its back by a Pneumatic PicoPump (PV800; World Precision Instruments) gated by a transistor-transistor logic pulse under software control. Pulse duration was 1–2 sec when measuring the voltage dependence of the ATP-evoked ion currents and 100 msec when monitoring rapid changes in intracellular [Ca^{2+}]. Under these experimental conditions all cells tested responded to ATP. Control experiments in which ATP was omitted from the solution in the puff pipette indicated that the contribution of mechanosensitive transduction currents was negligible. However, as a general precaution, care was taken to consistently orient ATP ejection in the inhibitory direction of mechanosensitivity.

Ca^{2+} fluorescence imaging. Fluorescence imaging of intracellular Ca^{2+} was performed as described in Mammano et al (1999). Briefly, light from a 75 W stabilized Xenon arc source (Cairn Research Ltd.) was coupled via a liquid light guide, gated by a rapid shutter (UniBlitz; Vincent Associates) to the epifluorescence section of a modular upright microscope (MI 250; Newport). An interference filter and a long-pass dichroic mirror (D480/30x and 505DCLP; Chroma Technology Corporation) were used to select a narrow range of excitation wavelengths around the absorption maximum of Calcium Green-1 (505 nm). Fluorescence emission was selected around 535 nm using a second pair of dichroic blade and interference filter (XF23; Omega Optical). The illumination intensity was attenuated with a diaphragm to avoid phototoxicity by reducing dye photo-bleaching rates to ≤0.5%/sec. The microscope was equipped with an infinity-corrected water-immersion objective (63×, NA 0.90; Achroplan, Carl Zeiss). An achromatic doublet was used as a projection lens to form fluorescence images on a fast (15 MHz readout rate) CCD sensor (IA-D1; DALSA, Ontario, Canada) that was cooled by a peltier device (Marlow Industries). The output of the sensor was digitized at 12 bits/pixel by customized electronics to produce 128 × 128 pixel images that were recorded in real time to the RAM of a host PC with a high-performance digital framegrabber (ICPCI/AM-DIG16; Imaging Technology) controlled by customized software. The timing of image capture was determined by sampling the frame-valid signal of the CCD sensor. Recorded images were saved to a UW-SCSI hard drive and analyzed off-line using routines developed from the Image Processing Toolbox of Matlab 5.1 (The Mathworks Inc.). For each image pixel, fluorescence signals were computed as ratios $\Delta F/F = [F(t) − F(0)]/F(0)$, where t is time, $F(t)$ is fluorescence after a stimulus that causes calcium elevation within the cell, and $F(0)$ is prestimulus fluorescence computed by averaging 10–20 images. Both $F(t)$ and $F(0)$ were corrected for mean background fluorescence computed from a 20 × 20 pixel rectangle devoid of obvious cellular structures. This local ratio computation is expected to provide correction for time-independent nonuniformity in optical path-length and dye concentration (Neher and Augustine, 1992). Finally, ratio magnitude was encoded by 8 bit pseudocolor look-up tables to produce pseudocolor images that were smoothed with a 3 × 3 two-dimensional median filter.

Motility measurement. Motility measurements were performed as described in Frolenkov et al (1997). Briefly, OHC movements were recorded with a video camera interfacing with an inverted microscope equipped with Differential Interference Contrast optics to an optical disk recorder (Panasonic TQ-3031F). Digitized images were analyzed off-line with the image-processing system Image 1 (Universal Imaging, West Chester, PA). For movement quantification, a measuring rectangle ranging in length from 5 to 10 μm and composed of 3–15 rows of pixels was positioned across the moving edge of the cell. The intensity of the image brightness (in arbitrary units) along these pixel lines was averaged, and the number of points in each raw intensity profile was increased 10× by cubic spline interpolation. Movements of the cell edge were calculated from the shifts, computed by a least-square procedure, in the interpolated intensity profiles. The sensitivity of the measurement was ~0.02 μm, as previously determined (Frolenkov et al., 1997).

Nonlinear capacitance measurement. Transient asymmetric currents were measured by rapidly changing the potential of isolated OHCs under

whole-cell patch-clamp recording conditions. Measurements of cell capacitance were derived from those of asymmetric currents evoked by prestepping the cell potential to large hyperpolarized values V_{pre}, around -160 mV, for ~1 msec from their resting potential V_r, followed by depolarizing steps of variable amplitude and 2–3 msec duration. The potential was then returned to V_{pre} for 2–3 msec before resetting it to V_r, preparing the cell for the next step. Charge movement Q was estimated by time-integration of the asymmetric currents at the step offset, when the cell was temporarily returned to V_{pre}, i.e., under constant driving-force conditions. Because the time constant of the patch-clamp amplifier was in the range 0.1–0.3 msec, >99.9% of the current had settled within 2 msec corresponding, in the worst case, to 6.6 time constants. Leakage currents were estimated and subtracted off-line by assuming that asymmetric currents had completely decayed at the end of the eliciting pulse. This procedure was found to introduce less noise than the standard P/4 technique (Armstrong and Bezanilla, 1977). In most cases, ionic currents were not activated appreciably during the brief voltage commands applied (Mammano and Ashmore, 1996). This was confirmed in test experiments using intracellular and extracellular solutions designed to block most of the voltage-dependent conductances of the OHCs. Data were normalized for differences in cell dimension by estimating the surface area of the lateral fraction of the membrane. Q–V relationships obtained in this way were fitted by scaled Boltzmann functions $Q(V) = Q_0\{1 + \exp[-(V - V_p)/W]\}^{-1}$. Here Q_0 (in femtocoulombs per square micrometer) is the maximum specific charge transferred, V_p the potential at which the charge is equally distributed, and $W = k_B T/ze$ a constant which is a measure of the charge displacement sensitivity to potential. It is expressed in terms of a moving charge of valence z translocating from the inner membrane surface to the outer, across the full membrane potential drop V. k_B is Boltzmann's constant, T is absolute temperature, and e the charge of the electron.

Immunofluorescence and electron microscopy. For immunofluorescence, guinea pig or rat cochleae ($n = 12$) were opened and fixed in 4% paraformaldehyde in PBS, pH 7.4, for 1 hr. Rat cochleae were used for the immunolocalization of InsP₃ receptors because of the species specificity of the antibody. Samples were permeabilized with 0.5% Triton X-100 in PBS for 30 min, followed by overnight incubation in blocking solution (5% goat serum plus 2% bovine serum albumin in PBS). Samples were incubated with 2.5 µg/ml of affinity-purified primary antibodies for 1 hr [the anti G$_\alpha$-protein antibody was obtained from DuPont (Billerica, MA), and the anti-InsP₃-receptor antibody was obtained from Calbiochem(La Jolla, CA)]. As a secondary antibody, we used FITC-conjugate anti-rabbit IgG (Amersham, Arlington Heights, IL). Samples were viewed with a Zeiss laser scanning confocal microscope or a Zeiss Axiophot microscope equipped with a 63× objective (NA, 1.4). No signal was detected when using the secondary antibody alone. For the G$_\alpha$-protein labeling, we also performed an additional control in which the primary antibody was preadsorbed for 1 hr at room temperature with an excess of the immunogenic peptide (50 µg/ml), which suppressed the labeling. For thin-section electron microscopy, organ of Corti samples were fixed using a reduced osmium method (Langford and Coggeshall, 1980) in order to enhance membrane contrast. In summary, the samples were initially fixed in 1.5% glutaraldehyde, 1.0% formaldehyde, and 0.08 M sodium cacodylate buffer, pH 7.2, with 2.5% sucrose for 2 hr at 4°C. After several buffer rinses, the tissues were then post-fixed in 1% osmium tetroxide and 1.5% potassium ferricyanide in cacodylate buffer for 1 hr. After several distilled water rinses, the samples were block-stained with uranyl acetate, dehydrated through an acetone series, then embedded and polymerized in Polybed 812 epoxy resin. For freeze-fracture, specimens were fixed for 2 hr by immersion in 2% glutaraldehyde and 2% paraformaldehyde in 0.1 M sodium cacodylate buffer solution, pH 7.2, rinsed in PBS, cryoprotected in 30% glycerol in PBS, and then frozen by immersion in liquid Freon 22. The frozen samples were fractured at $-120°C$ and replicated in a Balzers 301 apparatus. Electron micrographs were taken with a Zeiss 902 electron microscope.

RESULTS

Effects of ATP on the whole-cell currents

ATP-evoked currents and Ca²⁺ responses of OHCs were studied *in situ*, in a preparation of the isolated cochlea that preserved the structural integrity of the organ of Corti (Mammano et al., 1995). Figure 1*A*–*C* illustrates the experimental paradigm for these

recordings. Focal application of ATP at a distance of ~10 µm from the stereocilia evoked inward currents in OHCs that were voltage-clamped at potentials between -50 and -60 mV, near their mean resting potential V_r (-58 ± 4 mV; $n = 36$). A representative trace of a whole-cell current evoked by a 1 sec application of 50 µM ATP is shown (Fig. 1*C*, *top*). Currents of similar amplitude were evoked when ATP was applied for 100 msec (puff application) at a pipette concentration of 1 mM (Fig. 1*C*, *bottom*). The ATP-evoked currents did not show appreciable receptor desensitization even for prolonged applications (up to 10 sec, 50 µM; data not shown). Therefore, it was possible to determine the voltage dependence of the ATP-evoked currents by commanding the cell membrane potential to follow a ramp from -100 to $+30$ mV before the application of drug and during the peak of the response to 50 µM ATP applied for 1–2 sec (Fig. 1*D*). The reversal potential of the ATP-induced current was close to 0 mV (mean, $+2 \pm 3$ mV; $n = 12$), as previously reported (Nakagawa et al., 1990; Housley et al., 1992).

Simultaneous measurements of the ATP-evoked currents and [Ca²⁺]$_i$ responses

To reduce response variability (Raybould and Housley, 1997), measurements were performed on OHCs from the third row of the third cochlear turn that were 60–70 µm long. When the puff duration was 100 msec and the concentration of ATP in the pipette was 1 mM, the mean amplitude of the ATP-evoked current of the control sample was -692 ± 108 pA ($n = 8$). Currents appeared with a delay of 37 ± 4 msec from the puff onset, peaked in 90 ± 6 msec, decayed with variable rates (likely because of differences in the local fluid flow around the stereocilia within the perfusion chamber) and were accompanied throughout by an increase in [Ca²⁺]$_i$. At the apical pole of the cell, the Calcium Green-1 fluorescence change $\Delta F/F$ was maximal, and its rising time course was nearly exponential, with time constant $\tau_a = 469 \pm 42$ msec ($n = 8$); at the synaptic pole the time course was sigmoidal (Fig. 2*A,B*). The fluorescence responses at various positions along the cell axis were approximated by function,

$$F(t, x) = A\{1 - erf[x/(2(Dt)^{1/2}]\}:$$

which is a solution to the one-dimensional diffusion equation $\delta F/\delta t = D\, \delta^2 F/\delta x^2$ (Kevorkian, 1990), where t is time, x is position, $D = 220$ µm²/sec is the diffusion constant of Ca²⁺ in the cytoplasm (Allbritton et al., 1992), and A is an amplitude scale factor.

The black solid lines superimposed on the $\Delta F/F$ traces in Figure 2*B*, which were generated assuming $A = 30$ and (from top to bottom) $x = 8.5, 20.5, 32.5, 44.5, 56.5,$ and 68.5 µm as the position along the cell axis (measured from the base of the hair bundle), corresponds to the rapid establishment and subsequent relaxation of an intracellular gradient of [Ca²⁺]. The Ca²⁺ responses decreased with time after the first puff, being reduced by $50 \pm 23\%$ ($n = 3$) of the control after the third application of ATP, whereas the ATP-evoked currents decreased by $20 \pm 12\%$ (Fig. 2*C,D*). During this time, V_r shifted to more depolarized values, probably because of the activation by Ca²⁺ of nonselective cation channels (Abbeele et al., 1996). The involvement of L-type Ca²⁺-channels in the generation of these ATP-induced Ca²⁺ responses can be excluded because the associated conductance is activated at potentials more than or equal to -30 mV
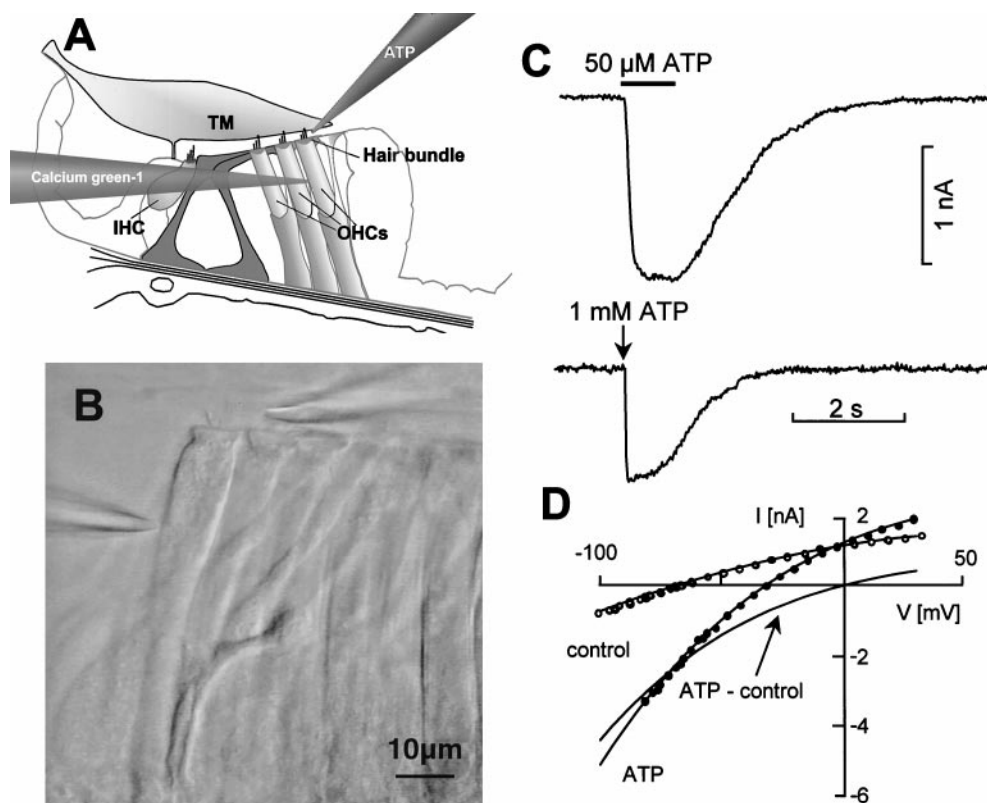
Figure 1. Patch clamping OHCs in the isolated cochlea. *A,* Schematic diagram of the organ of Corti showing the Calcium Green-1-filled patch pipette and the ATP-filled puff pipette. *TM, T*ectorial membrane; *IHC,* inner hair cells; *OHCs,* outer hair cells. *B,* Video image of row 3 OHCs showing the patch pipette entering from the *left* and sealed onto the lateral plasma membrane of an OHC; a puff pipette, entering from the *right,* was positioned in the proximity of the stereocilia for the focal pressure application of ATP. Scale bar, 10 μm. *C, Top,* Representative whole-cell current evoked by a 1 sec application of 50 μM ATP (*bar*). *Bottom,* Current evoked by a puff applied for 100 msec (*downward vertical arrow*) from a pipette loaded with 1 mM ATP. *D,* Current–voltage (*I–V*) relationship derived from 1 sec voltage ramps from −100 to +30 mV applied at the peak of the response to ATP (2 sec, 50 μM). Potentials were corrected for the drop caused by the access resistance (6.3 MΩ). *Solid lines* through data are least squares polynomial fits. The *solid line* intersecting the abscissa near 0 mV is the difference between fits and thus represents the ATP-sensitive fraction of the *I–V*.

(Chen et al., 1995); i.e., 20 mV more depolarized than the most positive holding potential used in our experiments.

Spatial localization and temporal resolution of the apical [Ca^{2+}]$_i$ rise

By increasing the secondary magnification of the microscope, the Ca^{2+} rise at the cell apex was found to have two distinct components. As shown in Figure 3*A*, ~92 msec after the onset of the ATP puff, i.e., by the time the inward current had peaked, focal fluorescence increase was detected at the top of the stereocilia and the cuticular plate. At 153 msec the whole hair bundle cytoplasm was filled with Ca^{2+}. The [Ca^{2+}]$_i$ maximum for this first component was reached at 259 msec. Figure 3*B* shows a 4–5 times larger component that started at ~0.6 sec, peaked at 2 sec, and localized to a region right below the cuticular plate, 3–10 μm from the apical surface. The different localization of these two successive [Ca^{2+}]$_i$ maxima and their temporal relationship to the whole-cell current are highlighted in Figure 3*C*.

Effects of extracellular Ca^{2+} removal

The two-component pattern of Ca^{2+} signaling suggested possible contributions from different subtypes of P2 receptors. Therefore we performed a set of experiments in which Ca^{2+} ions were transiently removed from the extracellular medium (0 [Ca^{2+}]$_o$). In 0 [Ca^{2+}]$_o$, both the ATP-evoked currents (−1933 ± 665 pA)

and the Ca^{2+} responses (58 ± 7% $\Delta F/F$) increased approximately threefold over the controls in standard 1.25 mM [Ca^{2+}]$_o$ (*n* = 3). The Calcium Green-1 fluorescence change (Fig. 4*A*) was again maximal at the apical pole of the cell, where it rose nearly exponentially with time constant τ_a = 1497 ± 174 msec, and followed a sigmoidal time course at the synaptic pole. The time course and the location of the $\Delta F/F$ response peak (Fig. 4*B*) indicated that the [Ca^{2+}]$_i$ rise in 0 [Ca^{2+}]$_o$ corresponded to the second component, observed when Ca^{2+} was present in the bathing medium, and that the fluorescence increase was caused by intracellular diffusion of Ca^{2+} after release from stores confined to the cell apex. OHCs were routinely tested for positive responses to ATP before applying pyridoxalphosphate-6-azophenyl-2′,4′-disulfonic acid (PPADS; 30 μM), a selective antagonist to P2 purinoceptors (Lambrecht et al., 1992). Both current and Ca^{2+} responses were completely suppressed by PPADS and did not recover after the control solution had been restored for up to 40 min (*n* = 3; data not shown).

Characterization of the Ca^{2+} release site and the signal transduction pathway

Ca^{2+}-mobilizing P2Y receptors couple via G-proteins to activate phosphoinositide-specific phospholipase C and produce InsP$_3$ (Linden, 1999). To determine the possible contribution of InsP$_3$-gated intracellular Ca^{2+} release to the $\Delta F/F$ fluorescence
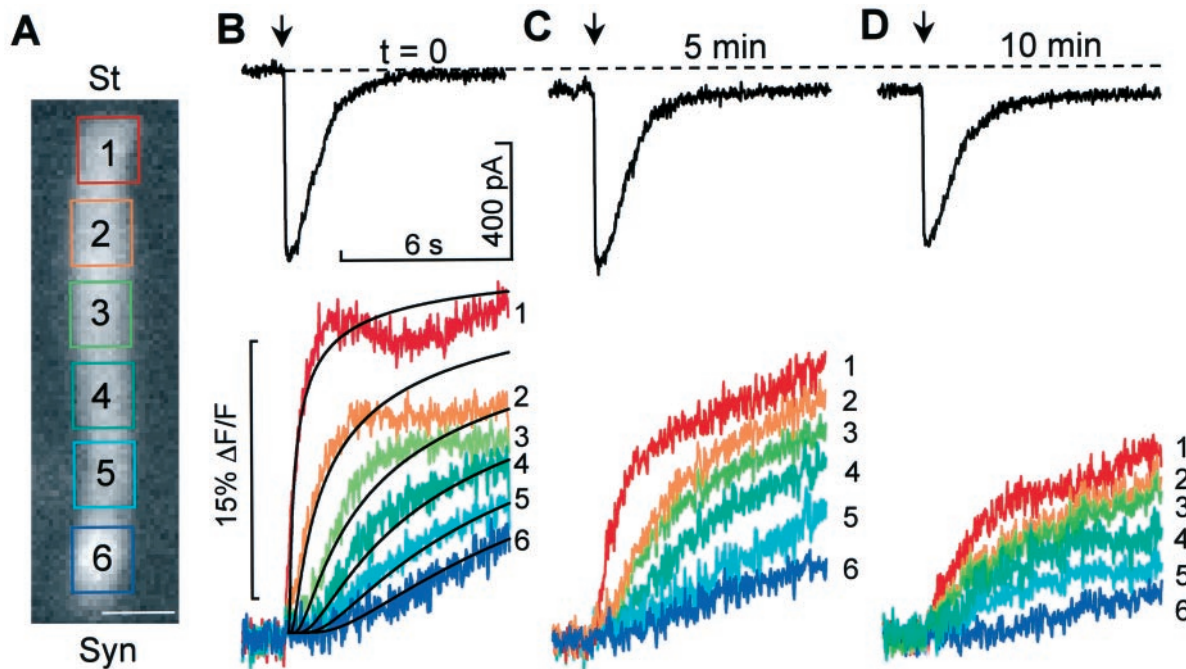
Figure 2. Simultaneous recording of ATP-evoked currents and Calcium Green-1 fluorescence from OHCs in the organ of Corti. *A,* Fluorescence image of an OHC with six superimposed rectangular regions of interest (ROIs) covering the cell body from stereocilial (*St*) to synaptic pole (*Syn*). Scale bar, 10 μm. *B, Top,* Whole-cell current evoked by the puff application of ATP (1 mM, 100 msec; *arrow*) to the stereocilia of the cell in *A*. *Bottom,* Corresponding fluorescence increases averaged over each of the six color-coded and number-coded ROIs. *Solid black lines* superimposed on fluorescence traces are solutions to the one-dimension diffusion equation, computed at various distances from the stereocilia base (see Materials and Methods). *C, D,* Applications of ATP to the same cell, repeated at the indicated time, measured from the onset of the first puff. Data from sequences of 990 images acquired at the rate of 107 frames/sec.

changes, OHCs were loaded with heparin, a specific inhibitor of the InsP$_3$ receptors (Berridge, 1993), through the patch pipette. In 0 [Ca^{2+}]$_o$ and with 7 mg/ml heparin in the pipette (Markram et al., 1995), the amplitude of the fluorescence changes (12 $\pm$ 3% $\Delta F/F$; $n = 3$) was reduced to <¼ of control (Fig. 5A; $p < 0.05$; paired t test).

In an immuofluorescence assay using an anti-InsP$_3$ receptor polyclonal antibody, we observed that InsP$_3$ receptors are highly expressed in the apical cytoplasm (Fig. 5B–D) just below the cuticular plate, where the labeling appeared as a punctuated pattern (Fig. 5C, *arrows*). Some fluorescence labeling was also detected at the cell cortex along the lateral wall (Fig. 5D), indicating that InsP$_3$ receptors are also expressed, albeit at a lower concentration, in the lateral subsurface cisternae of OHCs.

Conventional transmission electron microscopy showed that the region of the OHC cytoplasm where the intracellular store responsible for the Ca^{2+} release is located coincides with a distinct system of lamellar and tubulovesicular ER cisternae and mitochondria (Fig. 6A, *arrows*) named Hensen's body (Lim, 1986). By contrast, the middle region of the OHC cytoplasm contains very few organelles or cytoskeletal components. The freeze-fracture replicas in Figure 6, *B* and *C*, are close-up views of the Hensen's body, showing a whorl of concentric lamellar and tubulovesicular cisternae and associated mitochondria (*arrows*), with different degrees of fenestration.

We could not obtain direct immunofluorescence evidence for the presence and localization of P2Y receptors in the apical region of the OHC, because specific antibodies are not available. However, the use of an anti-peptide antibody that identifies the α

subunit of G-proteins revealed an intense labeling of the OHC stereocilia (Fig. 7A,B). This labeling was suppressed when we preabsorbed the antibody with the immunizing peptide (Fig. 7C).

Voltage-dependent capacitance and electrically evoked motile responses

We tested whether the localized ATP-dependent Ca^{2+}-release had an effect on the electromotility of isolated OHCs, using a different patch-clamp and video recording set-up. ATP was applied while monitoring both the voltage-driven cell shape changes and their electrical correlates: transient asymmetric currents (Gale and Ashmore, 1997) and nonlinear capacitance (Iwasa, 1997). In these experiments, nonlinear charge-displacement $Q(V)$ recordings (Fig. 8A) were obtained by time-integration of asymmetric currents evoked by brief depolarizing voltage steps in the range from -160 to $+100$ mV. Data were fitted by scaled Boltzmann functions. The mean $\pm$ 1 SE values of the Boltzmann parameters V_p, z, and Q_{max} (see Materials and Methods) for the controls were: -35 ± 7 mV; 0.79 ± 0.02 and 1.6 ± 0.2 fC/μm^2; and after ATP (applied for 1–2 sec; 50 μM) were: -41 ± 7 mV; 0.82 ± 0.02 and 1.5 ± 0.2 fC/μm^2. The half-activation potential of $Q(V)$, V_p, displayed a small, statistically significant (at $p = 0.05$ level) -6 mV shift after ATP, corresponding to a change of cell length of $\sim$100 nm, while the potential sensitivity, W, was not affected. Numerical differentiation of charge displacement data produced bell-shaped relationships between the specific capacitance, C, and the membrane potential, V. The asymptotic values of $C(V)$ for large positive and negative potentials approached 1 μF/cm^2, as expected for a lipid bilayer, whereas peak values were
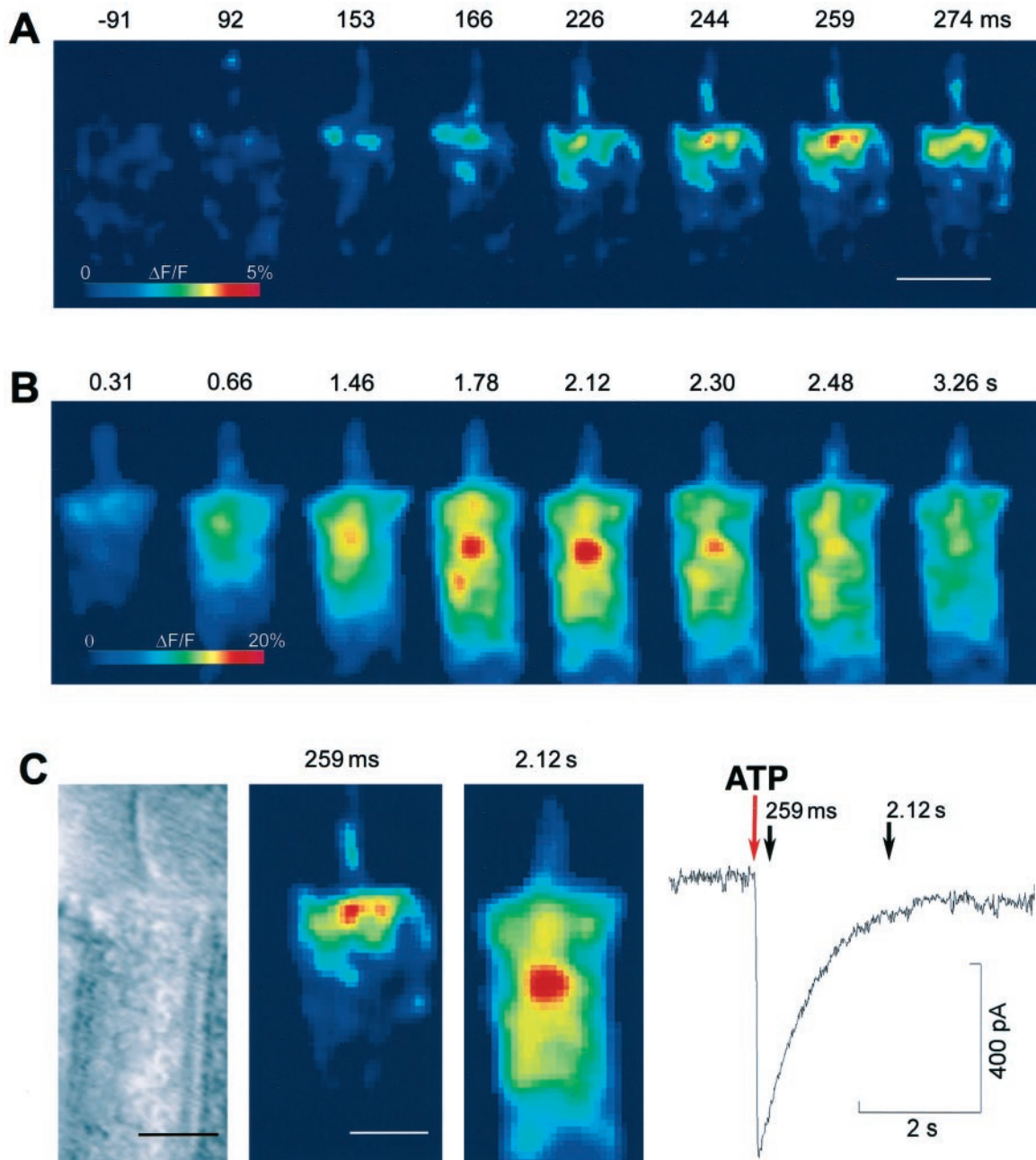
Figure 3. Ca^{2+} concentration changes at the OHC apical pole. *A,* Eight selected images from a sequence of 600 frames acquired at the rate of 66 frames/sec; numbers above each image are time in milliseconds from the onset of the ATP puff (1 mM, 100 msec). Notice focal Ca^{2+} elevation at the stereocilia and cuticular plate at 92 msec. The first response maximum is at 259 msec. Scale bar, 10 μm. *B,* Eight subsequent images from the same sequence, plotted with a different pseudocolor look-up table; numbers above each image are time in seconds from the puff onset. The second response maximum is at 2.12 sec. *C,* Comparison of the fluorescence images at the time of the two response maxima to a bright-field image of the same OHC, showing the different location of the $[Ca^{2+}]_i$ peaks relative to the cell apical surface. The trace to the *right* is the simultaneous ATP-evoked whole-cell current. The *red downward arrow* points to the time of puff application. The acquisition times of the two fluorescence images are marked by *black arrows.* Notice nearly complete decay of the current at 2.12 sec.

2.5 times larger as a consequence of the large polarization charge of the putative membrane motor protein (Iwasa, 1997). Figure 8*B* illustrates typical electromotile responses, measured simultaneously to the asymmetric currents, before (*circles*), during (*triangles*), and after (*squares*) applications of 50 μM ATP for 1 sec. Data were fitted by scaled negative Boltzmann functions. The average values of the Boltzmann parameters V_p, z, and A_o (see Materials and Methods) for four OHCs were, for the control:

-26 ± 9 mV; 0.88 ± 0.05, $3.3 \pm 0.5\%$; and after ATP: -28 ± 9 mV; 0.84 ± 0.03, $2.6 \pm 0.5\%$. Parameters A_o (amplitude scale factor, as percent units of cell length), V_p, and W did not vary significantly as a consequence of the ATP application. However, because motility measurements are generally affected by a larger cell-to-cell variability, this is not in contrast with the small V_p change characterizing the nonlinear charge-displacement recordings.
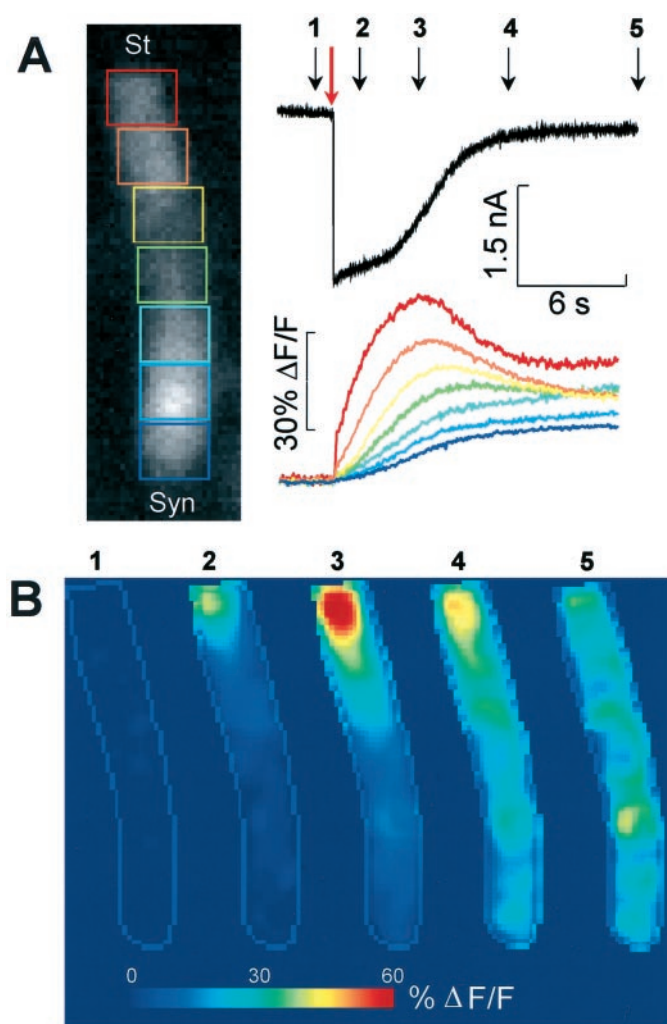
Figure 4. $[Ca^{2+}]_i$ surge induced by ATP in $0 [Ca^{2+}]_o$. *A, Top,* Whole-cell current evoked by a puff application of ATP (1 mM, 100 msec; *red arrow*). *Bottom,* Corresponding fluorescence increase measured from the seven color-coded rectangular ROIs shown. Dimension of ROIs: 10×8 μm. *B,* Five selected pseudocolor images generated from fluorescence images captured at the times marked by the *numbered black arrows* in *A.* Notice Ca²⁺ surge centered at ~5 μm below the apical surface of the cell. Sequence of 1050 frames; rate: 54 frames/sec.

DISCUSSION

The large noninactivating inward currents evoked by ATP are consistent with the profile of the ionotropic P2X₂ receptor subtype (Werner et al., 1996; Housley, 1997; Parker et al., 1998). On the other hand, this was neither the only nor the main source for the $[Ca^{2+}]_i$ increases because: (1) ATP potently mobilized intracellular Ca²⁺ in $0 [Ca^{2+}]_o$; and (2) this effect was inhibited by heparin, a drug extensively used as a competitive inhibitor of InsP₃-binding to InsP₃ receptors. The incomplete block of the Ca²⁺ responses in heparin-loaded OHCs (Fig. 5*A*) may be the consequence of limited diffusion of this heavy polyanion (MW, 6000–20,000) into the cell cytoplasm in the few minutes between the establishment of the whole-cell recording conditions and the beginning of the image acquisition. However, the complete suppression of the Ca²⁺ responses by PPADS in $0 [Ca^{2+}]_o$ is compatible with an intracellular signaling cascade activated by P2Y receptors, coupled via G-proteins to InsP₃ production and mobilization of intracellular Ca²⁺ (Brown et al., 1995; Lambre-

cht, 1996). Support for this assumption was provided by the immunolocalization of InsP₃ receptors to the apical OHC cytoplasm (Fig. 5). Immunolabeling with antibodies cross-reacting with a motif common to the α subunit of all G-proteins showed that a G-protein-coupled signaling system is present in the hair bundle of the OHCs (Fig. 7), which is a necessary albeit not sufficient condition for establishing the presence of metabotropic ATP receptors. When Ca²⁺ ions were removed from the bathing medium, whole-cell currents were augmented while $[Ca^{2+}]_i$ surged massively in the subcuticular region of the OHC cytoplasm (Fig. 4). The explanation of this seemingly paradoxical effect requires consideration of several interrelated facts. First, ATP-gated ion channels are partially blocked by Ca²⁺ (Housley, 1997). Therefore, Ca²⁺ removal is expected to facilitate the flow of ionic current across the apical surface of the cell (mostly Na⁺, with the solutions used; Housley et al., 1998). Secondly, divalent cations, such as Ca²⁺ and Mg²⁺, buffer ATP by binding to, and possibly reducing, the effective concentration of the agonist (Cockcroft and Gomperts, 1979). Thus, Ca²⁺ removal is expected to augment the response of the ionotropic P2X receptors, responsible for the generation of the increased inward currents, and the metabotropic P2Y receptors, responsible for the generation of the large Ca²⁺ signals in $0 [Ca^{2+}]_o$. Finally, the stationary level of cytosolic Ca²⁺ is lowered when $[Ca^{2+}]_o$ is decreased (Ashmore and Ohmori, 1990), and this may relieve, at least in part, the inhibitory action of $[Ca^{2+}]_i$ on the InsP₃-induced Ca²⁺ release (Pozzan et al., 1994; Putney, 1999). Besides by cytosolic Ca²⁺, InsP₃ receptors are regulated by ATP, pH, and phosphorylation (Bezprozvanny, 1995). Any of these factors may have changed during exposure of the cells to $0 [Ca^{2+}]_o$, resulting in a $3.2\times$ longer time constant of the apical $[Ca^{2+}]_i$ rise compared to the control in $1.25 [Ca^{2+}]_o$ (compare Figs. 2*B* and 4*A*).

The results obtained in $0 [Ca^{2+}]_o$ are likely to be more representative of the *in vivo* situation for: (1) $[Ca^{2+}]_o$ in the endolymph bathing the apical pole of the cell is low (23 μM; Wangemann and Schacht, 1996); (2) the resting level of $[Ca^{2+}]_i$ in OHCs *in situ* and *in vitro* is probably higher than *in vivo* because of unavoidable damage caused by the dissection procedure and prolonged exposure of the cell to millimolar levels of Ca²⁺ in the standard recording medium.

The decrease in the Ca²⁺ responses with multiple ATP applications exceeded that of the associated ATP-evoked currents (Fig. 2*B*–*D*). This could be caused by (1) the P2X and P2Y receptors exhibiting different degrees of desensitization, and/or (2) desensitization of the intracellular messenger receptors. However, a similar decrease has been reported for supporting cells of the organ of Corti (Dulon et al., 1993) and for inner hair cells (Sugasawa et al., 1996), even under perforated-patch conditions that should have better preserved the native constituents of the cytoplasm. Thus, the decrease could more simply be the consequence of Ca²⁺ release from intracellular stores unable to refill under these experimental conditions.

The structural correlates of the Ca²⁺ release

The increase of $[Ca^{2+}]_i$, after the application of extracellular ATP to isolated hair cells and supporting cells of the auditory and vestibular sensory neuroepithelia of the chick and the guinea pig *in vitro*, has been attributed both to intracellular and extracellular sources (Ashmore and Ohmori, 1990; Shigemoto and Ohmori, 1990; Dulon et al., 1991, 1993; Rennie and Ashmore, 1993; Nilles et al., 1994; Sugasawa et al., 1996). However, these studies lacked the spatial and temporal resolution necessary to clearly identify a
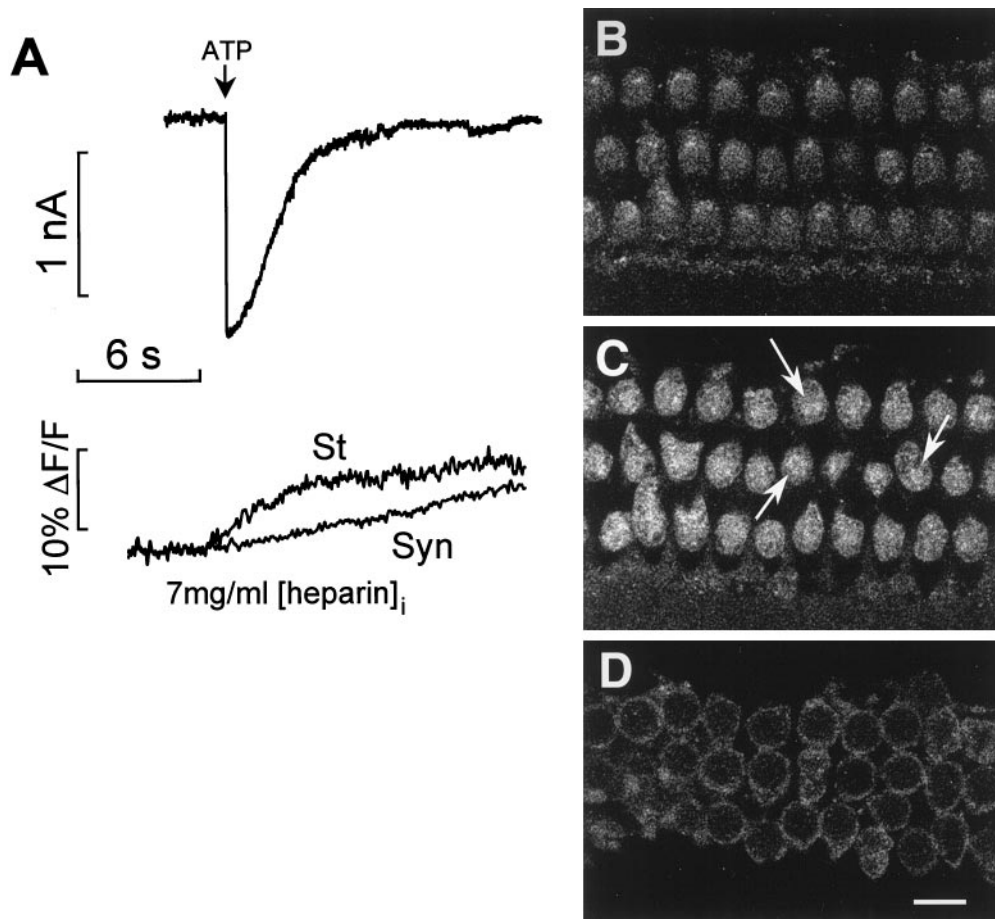
Figure 5. Inhibition by heparin and immunolocalization of InsP₃ receptors. *A,* Effect of intracellular heparin (7 mg/ml) on Ca²⁺ movement. *Top,* Current evoked by ATP (1 mM, 100 msec); *bottom,* corresponding fluorescence changes measured in 0 [Ca²⁺]ₒ from a region adjacent to the OHC cuticular plate (*St*) and near the synaptic pole (*Syn*). *B—D,* Confocal microscopy of ~0.4 μm cross-sections at 2, 7, and 20 μm below the apical surface of the three rows of OHCs from a whole-mount preparation of the organ of Corti, labeled with the anti-InsP₃ receptor antibody. Intense fluorescence was observed just below the cuticular plate (*C*). Some fluorescence labeling was also detected at the cell cortex along the lateral wall, forming the ring images in *D*. Scale bar, 10 μm.

subcellular structure as a candidate site for the intracellular Ca²⁺ release. Our results indicate that the prevalent effect of ATP on [Ca²⁺]ᵢ increase in guinea pig OHCs stems from release of Ca²⁺ from a cytoplasmic region just below the cuticular plate, at the base of the hair bundle. This region contains a whorl of tubulovesicular and cisternal ER and densely packed mitochondria forming a distinct structure, the Hensen's body (Lim, 1986), that is and has long been known, although it has no established functional role. It remains to be established whether also other hair cell types posses an ER that functions as a store of releasable Ca²⁺.

The involvement of specialized portions of ER in InsP₃-gated Ca²⁺ release has been observed in excitable and nonexcitable cells, such as hepatocytes and Purkinje neurons (for review, see Pozzan et al., 1994). In OHCs, the InsP₃-receptor labeling and the localization of the Ca²⁺ release to the subcuticular cytoplasm suggest that the Hensen's body might function as an InsP₃-sensitive Ca²⁺ storage compartment. The mitochondria associated with the Hensen's body could have a complementary function. Mitochondria have been shown in other cells to be a major sink for Ca²⁺ clearance when [Ca²⁺]ᵢ rises into the low micromolar levels (Rizzuto et al., 1993). Slow export from mitochondria can extend the period during which [Ca²⁺]ᵢ remains modestly elevated (150–500 nM), prolonging the period of activation

of Ca²⁺-dependent enzymes (for review, see Babcock and Hille, 1998).

Ca²⁺ compartmentalization and the insensitivity of electromotility to ATP

The OHC electromotility machinery is distributed along the entire lateral plasma membrane (Kalinec et al., 1992). Recently, it has been shown that acetylcholine increases electromotility in isolated OHCs by elevating [Ca²⁺]ᵢ (Dallos et al., 1997). However, an important feature of intracellular Ca²⁺ signaling is the spatial organization of the [Ca²⁺]ᵢ changes. Here we have found that the ATP-induced [Ca²⁺]ᵢ variations at the cell apex do not significantly influence electromotility (Fig. 8). Localized high levels of [Ca²⁺]ᵢ in the proximity of Ca²⁺ release sites have been implicated in the selective activation of specific processes, despite the eventual spread of the [Ca²⁺]ᵢ increase, which depends on the cell buffering power, to more distal parts of the cell (Rizzuto et al., 1993). Hair cells, and more specifically OHCs, are known to contain a large number of highly expressed Ca²⁺ binding proteins (Pack and Slepecky, 1995; Nomiya et al., 1998) that exert a spatial buffering of Ca²⁺, restricting the region of focal [Ca²⁺]ᵢ elevation (Roberts, 1993; Hall et al., 1997). Partial loss of these proteins caused by dialysis under whole-cell patch-clamp condi-
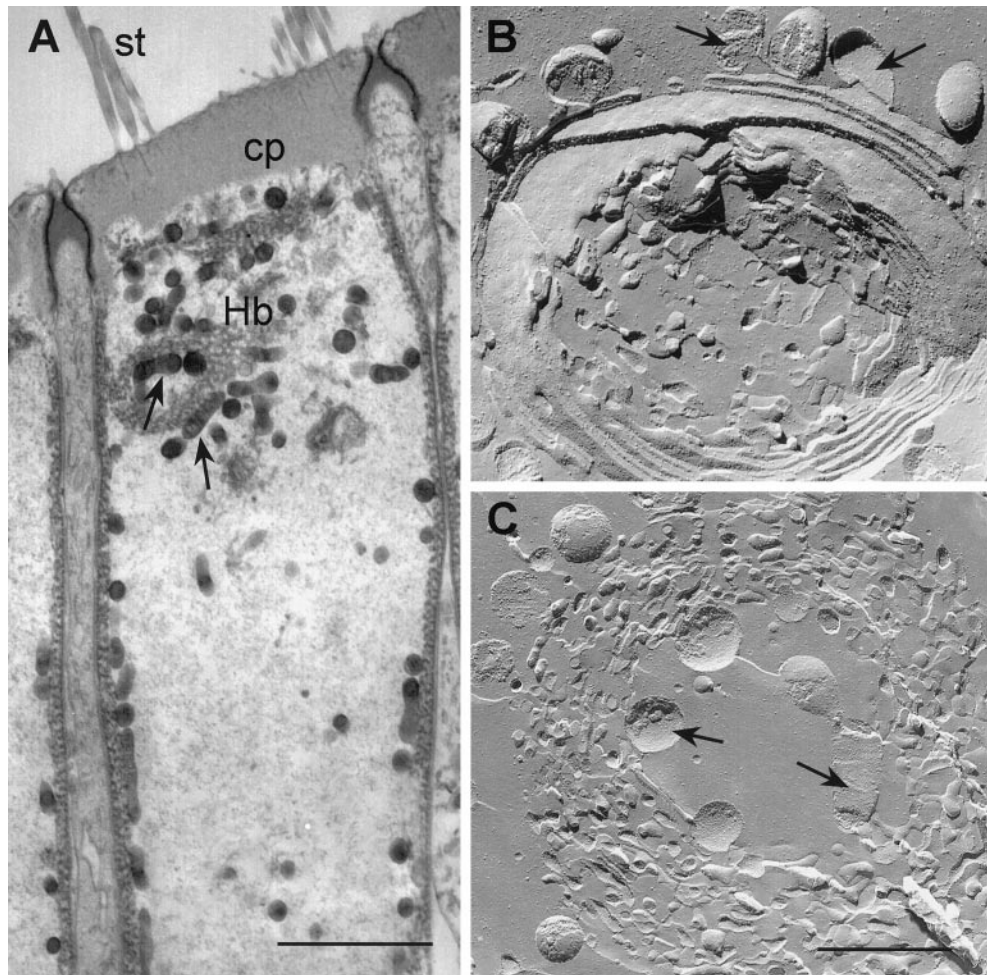
Figure 6. Ultrastructural characterization of the Ca^{2+} release site. *A,* Longitudinal thin section electron microscopy along the top half of the cylindrical cell body of an OHC. The stereocilia (*st*) insert in the dense actin-based filament matrix of the cuticular plate (*cp*), which is surrounded by the tight/adherens junction complex and together form the transcellular structure named reticular lamina (Fig. 1*A*). The Hensen's body (*Hb*), a whorl of lamellar and tubulovesicular cisternal ER and associated mitochondria (*arrows*), is characteristically present in the apical cytoplasm right below the cuticular plate. Subsurface cisternae and mitochondria underlie the whole length of the lateral plasma membrane of the OHC. The middle region of the cylindrical cell body contains very few organelles or cytoskeletal components. Scale bar, 5 µm. *B, C,* Freeze-fracture replica close-up views of the Hensen's body from two OHCs showing the mitochondria (*arrows*) and the whorl of ER cisternae with different degrees of fenestration. Scale bar, 1 µm.

tions facilitates the diffusion of the free Ca^{2+}. Therefore the spatial confinement of the ATP-dependent [Ca^{2+}]$_i$ surge to the apical pole of the cell is expected to be even more pronounced under physiological conditions. This localized Ca^{2+} increase is likely to subserve local functions related to the adjacent hair bundle structures.

Control of mechanosensory transduction by ATP

Ca^{2+} entry through the mechanosensitive channels in the stereocilia of hair cells has been shown to serve as a feedback signal in the adaptation process that sets the channel open-probability (Lumpkin et al., 1997). Moreover, the intracellular binding of Ca^{2+} to these channels has been posited to promote the increase of tension in the putative channel-gating springs (Markin and Hudspeth, 1995) that might underlie the active bundle movements observed in some vertebrate hair cells (Crawford and Fettiplace, 1985; Assad and Corey, 1992; Choe et al., 1998). However, Ca^{2+} is rapidly and effectively cleared from the stereocilia after entry through mechanosensory channels (Crouch and Schulte, 1995; Apicella et al., 1997; Burlacu et al., 1997; Ricci et al., 1998; Yamoha et al., 1998), which severely limits the spread of

Ca^{2+} to the lower segment of the hair bundle (Lumpkin and Hudspeth, 1998).

The stereocilia and the cuticular plate at the base of the hair bundle are supported by dense actin-based networks cross-linked by several unconventional myosin isozymes and actin-binding proteins (Hasson et al., 1997). Identification of genes responsible for deafness has revealed that novel myosin isoforms and other actin-binding proteins in the hair bundle are essential for inner ear function. For example, it has been shown that myosin-VIIa (Hasson et al., 1997) and myosin 15 (Probst et al., 1998) are required for maintaining the structural integrity of the bundle and for the assembly of the stereocilia into an ordered array, whereas myosin-VI participates in anchoring the stereociliary rootlets to the actin meshwork of the cuticular plate (Hasson et al., 1997). In addition, myosin 1β is found in the stereocilia and in the pericuticular necklace (Hasson et al., 1997).

The functions of several actin-binding proteins and myosin isozymes are known to be regulated by Ca^{2+}. Also, the structural and mechanical properties of actin networks containing actin-binding proteins and myosins, such as the leading lamella in
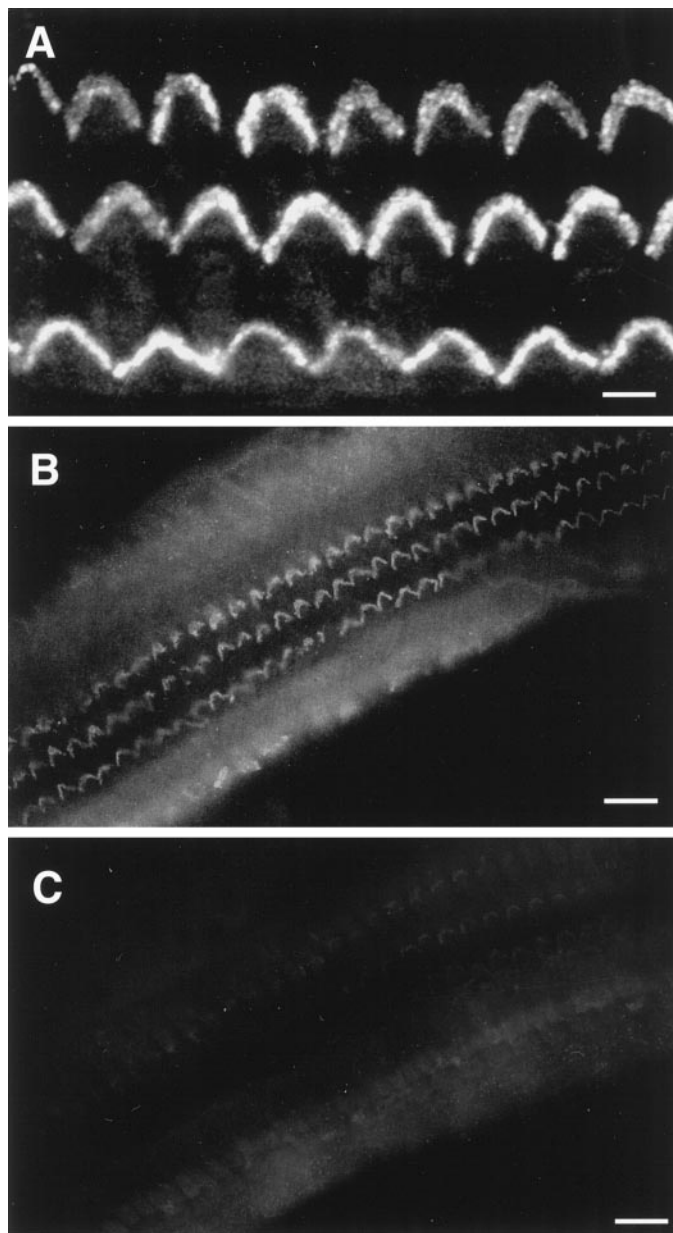
Figure 7. Immunolocalization of a G-protein to the stereocilia of OHCs. *A,* Fluorescence optical section obtained by confocal microscopy at the level of the hair bundle of the three rows of OHCs in a whole-mount preparation, immunolabeled with an antibody raised against an epitope common to the α subunit of all G-proteins, showing labeling of the stereocilia. *B, C,* Conventional fluorescence micrographs of the OHC hair bundles showing the immunolabeling reaction with the same affinity-purified antibody (*B*) and its suppression (*C*) when the antibody was preadsorbed with the immunizing peptide. Scale bars: *A,* 5 μm; *B, C,* 25 μm.
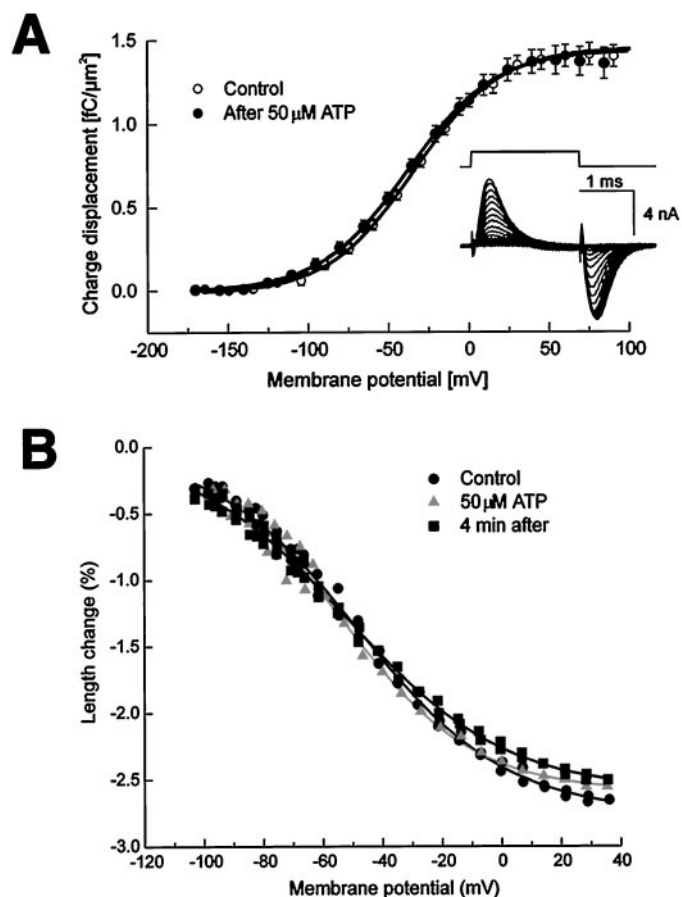

Figure 8. Voltage dependence of charge displacement and cell motility. *A,* Asymmetry charge displacement before (*open symbols*) and 5 min after the focal application of ATP (50 μM, 1–2 sec) to the stereocilia (*closed symbols*). Data are an average from six cells, normalized for lateral membrane surface area. Sigmoidal continuous lines are Boltzmann fits. *Inset* shows a typical set of leak-subtracted asymmetric currents. Voltage commands are displayed above current traces. *B,* Length changes measured from a representative OHC under voltage clamp. The holding potential was −60 mV. Membrane potential was commanded to follow a voltage ramp from −110 to +40 mV (corrected for access resistance) while recording a sequence of images at standard video rate. The OHC length was determined before (*circles*), during (*triangles*), and 4 min after (*squares*) ATP. *Solid lines* are Boltzmann fits.

motile cells, growth cones in neuronal cells, or the brush border of epithelial cells (which are analogous to the hair bundle actin networks) are known to be sensitive to Ca^{2+} (Regehr and Tank, 1994). Our results and our hypothesis, that the highly diffusible InsP$_3$ (Allbritton et al., 1992) is the second messenger for the release of intracellular Ca^{2+} in OHCs, suggest that, by elevating [Ca^{2+}]$_i$ at the base of the hair bundle, ATP would effectively bypass the efficient Ca^{2+}-clearance mechanisms of the stereocilia. Ca^{2+} released at this strategic location could potentially modulate the action of unconventional myosin isozymes and acting-binding proteins involved in maintaining the hair bundle integrity and potentially influence mechanotransduction. For example, the hair bundle of OHCs, in addition to its role in mechanosensory transduction, serves to mechanically couple the apical surface of the organ of Corti, i.e., the reticular lamina, to the tectorial membrane (Fig. 1*A*). Under physiological conditions, the reticular lamina oscillates not more than a few nanometers (Nobili and Mammano, 1996). Thus, even subtle changes either in the geometry or in the stiffness of the bundle, e.g., after a [Ca^{2+}]$_i$ increase, could influence the micromechanics of this coupling, affecting the resonance frequency of the tectorial membrane and the oscillation of the organ of Corti.

REFERENCES

Abbeele Van Den T, Tran Ba Huy P, Teulon J (1996) Modulation by purines of calcium-activated non-selective cation channels in the outer hair cells of the guinea-pig cochlea. J Physiol (Lond) 494:77–89.

Allbritton NL, Meyer T, Stryer L (1992) Range of messenger action of calcium ion and inositol 1,4,5-trisphosphate. Science 258:1812–1815.

Apicella S, Chen S, Bing R, Peninston JT, Llinas R, Hillman DE (1997) Plasmalemmal ATPase calcium pump localizes to inner and outer hair cell bundles. Neuroscience 79:1145–1151.

Armstrong CM, Bezanilla F (1977) Inactivation of the sodium channel. II. Gating current experiments. J Gen Physiol 70:567–590.

Ashmore JF, Ohmori H (1990) Control of intracellular calcium by ATP in isolated outer hair cells of the guinea pig cochlea. J Physiol (Lond) 428:109–131.

Assad JA, Corey DP (1992) An active motor model for adaptation by vertebrate hair cells. J Neurosci 12:3291–3309.

Babcock DF, Hille B (1998) Mitochondrial oversights of cellular Ca²⁺ signaling. Curr Opin Neurobiol 8:398–404.

Berridge MJ (1993) Inositol trisphosphate and calcium signaling. Nature 361:315–325.

Bezprozvanny IB (1995) Inositol (1,4,5)-trisphophate receptors: functional properties, modulation and role in calcium wave propagation. In: Organellar ion channels and transporters. Society for general physiologists series, Vol 51, (Clapham DE, Ehrlich B, eds), pp 75–86. New York: The Rockefeller UP.

Brown C, Tanna B, Boarder MR (1995) PPADS: an antagonist at endothelial P2Y-purinoceptors but not P2U-purinoceptors. Br J Pharmacol 116:2413–2416.

Burlacu S, Tap WD, Lumpkin, EA, Hudspeth AJ (1997) ATP-ase activity of myosin in hair bundles of the bullfrog's sacculus. Biophys J 72:263–271.

Chabbert C, Geleoc G, Lehouelleur J, Sans A (1994) Intracellular calcium variations evoked by mechanical stimulation of mammalian isolated vestibular type I hair cells. Pflügers Arch 427:162–168.

Chen C, Nenov A, Norris CH, Bobbin RP (1995) ATP modulation of L-type calcium channel currents in guinea pig outer hair cells. Hear Res 86:25–33.

Choe Y, Magnasco MO, Hudspeth AJ (1998) A model for amplification of hair bundle motion by cyclical binding of Ca²⁺ to mechanoelectrical-transduction channels. Proc Natl Acad Sci USA 95:15321–15326.

Cockcroft S, Gomperts BD (1979) Activation and inhibition of Calcium-dependent histamine secretion by ATP ions applied to rat mast cells. J Physiol (Lond) 296:229–243.

Crawford AC, Fettiplace R (1985) The mechanical properties of ciliary bundles of turtle hair cells. J Physiol (Lond) 364:359–379.

Crouch JJ, Schulte BA (1995) Expression of plasma membrane Ca-ATPase in the adult and developing gerbil cochlea. Hear Res 92:112–119.

Dallos P, He DZZ, Sziklai I, Metha S, Evans BN (1997) Acetylcholine, outer hair cell electromotility, and the cochlear amplifier. J Neurosci 17:2212–2226.

Dulon D, Mollard P, Aran J-M (1991) Extracellular ATP elevates cytosolic Ca²⁺ in cochlear inner hair cells. NeuroReport 2:69–72.

Dulon D, Moataz R, Mollard P (1993) Characterization of Ca²⁺ signals generated by extracellular nucleotides in supporting cells of the organ of Corti. Cell Calcium 14:245–254.

Frolenkov GI, Kalinec F, Tavartkiladze GA, Kachar B (1997) Cochlear outer hair cell bending in an external electric field. Biophys J 73:1665–1672.

Frolenkov GI, Atzori M, Kalinec F, Mammano F, Kachar B (1998) The membrane-based mechanism of cell motility in cochlear outer hair cells. Mol Biol Cell 9:1961–1968.

Gale JE, Ashmore JF (1997) An intrinsic frequency limit to the cochlear amplifier. Nature 389:63–66.

Hall JD, Betarbet S, Jaramillo F (1997) Endogenous buffers limit the spread of free calcium in hair cells. Biophys J 73:1243–1252.

Hasson T, Gillespie PG, Garcia JA, MacDonald RB, Zhao Y, Yee AG, Mooseker MS, Corey DP (1997) Unconventional myosins in inner-ear sensory epithelia. J Cell Biol 137:1287–1307.

Housley GD (1997) Extracellular nucleotide signaling in the inner ear. Mol Neurobiol 16:21–48.

Housley GD, Greenwood D, Ashmore JF (1992) Localisation of cholinergic and purinergic receptors on outer hair cells isolated from the guinea pig cochlea. Proc R Soc Lond B Biol Sci 249:265–273.

Housley GD, Raybould NP, Thorne PR (1998) Fluorescence imaging of Na⁺ influx via P2X receptors in cochlear hair cells. Hear Res 119:1–13.

Hudspeth AJ (1997) Mechanical amplification of stimuli by hair cells. Curr Opin Neurobiol 7:480–486.

Iwasa K (1997) Current noise spectrum and capacitance due to the membrane motor of the outer hair cell: theory. Biophys J 73:2965–2971.

Kachar B, Brownell WE, Altschuler R, Fex J (1986) Electrokinetic shape changes of cochlear outer hair cells. Nature 322:365–368.

Kalinec F, Holley MC, Iwasa KH, Lim DJ, Kachar B (1992) A membrane-based force generation mechanisms in auditory sensory cells. Proc Natl Acad Sci USA 89:8671–8675.

Kevorkian J (1990) Partial differential equations: analytical solutions techniques, pp 1–47. Pacific Grove, CA: Wadsworth & Brooks/Cole Mathematics Series.

Kirk DL, Yates GK (1998) ATP in endolymph enhances electrically-evoked oto-acoustic emissions from the guinea pig cochlea. Neurosci Lett 250:149–152.

Lambrecht G (1996) Design and pharmacology of selective P2-purinoceptor antagonists. J Auton Pharmacol 16:341–344.

Lambrecht G, Friebe T, Grimm U, Windscheif U, Bungardt E, Hildebrandt C, Baumert HG, Spatz-Kumbel G, Mutschler E (1992) PPADS, a novel functionally selective antagonist of P2 purinoceptor-mediated responses. Eur J Pharmacol 217:217–219.

Langford LA, Coggeshall RE (1980) The use of potassium ferricyanide in neural fixation. Anat Record 197:297–303.

Lim DJ (1986) Functional structure of the organ of Corti: a review. Hear Res 22:117–146.

Linden JM (1999) Purinergic systems. In: Basic neurochemistry: molecular, cellular and medical aspects, Ed 6 (Siegel GJ, Agranoff BW, Albers RW, Fisher SK, Uhler MD, eds), pp 347–362. Philadelphia, PA: Lippincott-Raven.

Lumpkin EA, Hudspeth AJ (1998) Regulation of free Ca²⁺ concentration in hair cell stereocilia. J Neurosci 18:6300–6318.

Lumpkin EA, Marquis RE, Hudspeth AJ (1997) The selectivity of the hair cell's mechanoelectrical-transduction channel promotes Ca²⁺ flux at low Ca²⁺ concentrations. Proc Natl Acad Sci USA 94:10997–11002.

Mammano F, Ashmore JF (1996) Differential expression of outer hair cell potassium currents in the isolated cochlea of the guinea pig. J Physiol (Lond) 496:639–646.

Mammano F, Kros CJ, Ashmore JF (1995) Patch-clamped responses from outer hair cells in the intact adult organ of Corti. Pflügers Arch 430:745–750.

Mammano F, Canepari M, Capello G, Ijaduola RB, Cunei A, Ying L, Fratnik F, Colavita A (1999) An optical recording system based on a fast CCD sensor for biological imaging. Cell Calcium 25:115–123.

Markin VS, Hudspeth AJ (1995) Gating-spring models of mechanoelectrical transduction by hair cells of the internal ear. Annu Rev Biophys Biomol Struct 24:59–83.

Markram H, Helm PJ, Sakmann B (1995) Dendritic calcium transients evoked by single back-propagating action potentials in rat neocortical pyramidal neurons. J Physiol (Lond) 485:1–20.

Mockett BG, Housley GD, Thorne PR (1994) Fluorescence imaging of extracellular purinergic receptor sites and putative ecto-ATPase sites on isolated cochlear hair cells. J Neurosci 14:6992–7007.

Muñoz DJB, Thorne PR, Housley GD, Billett TE, Battersby J (1995) Extracellular adenosine 5′-triphosphate (ATP) in the endolymphatic compartment influences cochlear function. Hear Res 90:106–118.

Nakagawa T, Akaike N, Kimitzuki T, Komune S, Arima T (1990) ATP-induced current in isolated outer hair cells of guinea pig cochlea. J Neurophysiol 63:1068–1074.

Neher E, Augustine GJ (1992) Calcium gradients and buffers in bovine chromaffin cells. J Physiol (Lond) 450:273–301.

Niedzielski AS, Schacht J (1992) P2 purinoceptors stimulate inositol phosphate release in the organ of Corti. NeuroReport 3:273–275.

Nilles R, Jarlebark L, Zenner HP, Heilbronn E (1994) ATP-induced cytoplasmic [Ca²⁺] increases in isolated cochlear outer hair cells. Involved receptor and channel mechanisms. Hear Res 73:27–34.

Nobili R, Mammano F (1996) Biophysics of the cochlea. II. Steady-state nonlinear phenomena. J Acoust Soc Am 99:2244–2255.

Nomiya S, Nishizaki K, Anniko M, Karita K, Ogawa T, Masuda, Y (1998) Appearance and distribution of two Ca²⁺-binding proteins during development of the cochlea in the musk shrew. Dev Brain Res 110:7–19.

Pack AK, Slepecky NB (1995) Cytoskeletal and calcium-binding proteins in the mammalian organ of Corti: cell type-specific proteins displaying longitudinal and radial gradients. Hear Res 91:119–135.

Parker MS, Larroque ML, Campbell JN, Bobbin RP, Deininger PL (1998) Novel variant of the P2X₂ ATP receptor from the guinea pig organ of Corti. Hear Res 121:62–70.

Pozzan T, Rizzuto R, Volpe P, Meldolesi J (1994) Molecular and cellular physiology of intracellular calcium stores. Physiol Rev 74:595–636.

Probst FJ, Fridell RA, Raphael Y, Saunders TL, Wang A, Liang Y, Morell RJ, Touchman JW, Lyons RH, Noben-Trauth K, Friedman TB, Camper SA (1998) Correction of deafness in shaker-2 mice by an unconventional myosin in a BAC transgene. Science 280:1444–1447.

Putney JW (1999) Calcium. In: Basic neurochemistry: molecular, cellular and medical aspects, Ed 6 (Siegel GJ, Agranoff BW, Albers RW, Fisher SK, Uhler MD, eds), pp 453–469. Philadelphia: Lippincott-Raven.

Raybould NP, Housley GD (1997) Variation in expression of the outer hair cell P2X receptor conductance along the guinea-pig cochlea. J Physiol (Lond) 498:717–727.

Regehr WG, Tank DW (1994) Dendritic calcium dynamics. Curr Opin Neurobiol 4:373–382.

Rennie KJ, Ashmore JF (1993) Effects of extracellular ATP on hair cells isolated from the guinea-pig semicircular canals. Neurosci Lett 160:185–189.

Ricci A, Fettiplace R (1998) Calcium permeation of the turtle hair cell mechanotransducer channel and its relation to the composition of endolymph. J Physiol (Lond) 506:159–173.

Ricci AJ, Wu YC, Fettiplace R (1998) The endogenous calcium buffer and the time-course of transducer adaptation in auditory hair cells. J Neurosci 18:8261–8277.

Rizzuto R, Brini M, Murgia M, Pozzan T (1993) Microdomains with high Ca²⁺ close to IP₃-sensitive channels that are sensed by neighboring mitochondria. Science 262:744–747.

Roberts WM (1993) Spatial calcium buffering in hair cells. Nature 363:74–76.

Shigemoto T, Ohmori H (1990) Muscarinic agonists and ATP increase the intracellular Ca²⁺ concentration in chick cochlear hair cells. J Physiol (Lond) 420:127–148.

Skellett RA, Chen C, Fallon M, Nenov AP, Bobbin RP (1997) Pharmacological evidence that endogenous ATP modulates cochlear mechanics. Hear Res 111:42–54.

Sugasawa M, Erostegui C, Blanchet C, Dulon D (1996) ATP activates non-selective cationic channels and calcium release in inner hair cells of the guinea-pig cochlea. J Physiol (Lond) 491:707–718.

Wangemann P, Schacht J (1996) Homeostatic mechanisms in the cochlea. In: The cochlea (Dallos P, Popper AN, Fay RR, eds), pp 149–164. New York: Springer.

Werner P, Seward EP, Buell GN, North RA (1996) Domains of P2X receptors involved in desensitization. Proc Natl Acad Sci USA 93:15485–15490.

Yamoha EN, Lumpkin EA, Dumont RA, Smith PJS, Hudspeth AJ, Gillespie PG (1998) Plasma membrane Ca²⁺-ATPase extrudes Ca²⁺ from hair cell stereocilia. J Neurosci 18:610–624.